Tomographic reconstruction of stress from photoelastic measurements using elastic regularization.

Szotten, David and Lionheart,
William RB and Tomlinson, Rachel A

2006

MIMS EPrint: **2006.5**

Manchester Institute for Mathematical Sciences
School of Mathematics

The University of Manchester

Reports available from: http://eprints.maths.manchester.ac.uk/
And by contacting: The MIMS Secretary
School of Mathematics
The University of Manchester
Manchester, M13 9PL, UK

ISSN 1749-9097

Tomographic reconstruction of stress from photoelastic measurements using elastic regularization.

D Szotten†, WRB Lionheart†§, RA Tomlinson‡

† School of Mathematics, University of Manchester, PO Box 88 Sackville St, Manchester, M60 1QD, UK, E-mail bill.lionheart@manchester.ac.uk

‡ Department of Mechanical Engineering, University of Sheffield, Mappin Street, Sheffield, S1 3JD, UK, email r.a.tomlinson@sheffield.ac.uk

Abstract. In this paper we consider the problem of recovering the stress tensor field of a three dimensional object from measurements of the polarization state of transmitted light. In contrast to the ray transform approach suggested by Sharafutdinov, which uses the inversion of planar Radon transforms to recover a single component of the deviatoric stress normal to a plane, we study the simultaneous reconstruction of all components of the deviatoric stress in each voxel using a matrix approximation to the truncated transverse ray transform. This approach allows us employ partial differential operators related to linear elasticity in a regularizing penalty term resulting in a well posed problem. We note that the hydrostatic stress is determined by the deviatoric stress (up to an additive constant) from the equilibrium equation, and that our numerical results confirm that the full stress tensor can be recovered using elastic regularization.

MSC 53C65, 44A12, 65R10

PACS numbers: 42.25.Lc, 42.30.Wb, 62.20.Dc

Submitted to: *Inverse Problems*

§ To whom correspondence should be addressed.

1. Introduction

Anisotropic inverse boundary value problems for Maxwell's equations are among the most challenging problems in our area from both a practical and theoretical perspective. An important class of examples is the case where permittivity and permeability are anisotropic (and are not a scalar multiple of each other), and the electromagnetic response is known at the boundary of a closed domain for a single frequency of excitation. There is at present no uniqueness theory for such problems and nor constructive inversion procedures known. Anisotropy in electromagnetics can arise in a number of ways in practical problems the most common being an effective anisotropic media as a homogenization limit of a layered or fibrous material, a crystalline or liquid crystal structure, or the result of a distortion of an isotropic medium. In this paper the cause of the anisotropy is the latter: an isotropic homogeneous elastic transparent medium has been subjected to a small distortion resulting in an anisotropic permittivity tensor, while the permeability remains isotropic and homogeneous. The problem is further simplified by the assumption that the deviation in the permittivity from the original homogeneous isotropic permittivity is sufficiently small to justify a ray transform approximation to Maxwell's equations, and a linear approximation to the dependence of the measured data on the permittivity, as detailed in the seminal work of Sharafutdinov [2].

This application is motivated by the practical problem of photoelastic tomography. In mechanical engineering it is necessary to predict the stress in a solid component under known loads. Currently it is common practice to construct a finite element (FE) model of the component and solve the finite element approximation to the partial differential equations of linear elasticity with known forces or displacements as boundary conditions. A limitation of FE (or indeed finite difference or finite volume) methods is that the method fails at singularities in the displacement field, such as crack tips. If the location of a singularity is known a priori it can be included in the model using special elements, but a continuous approximation will underestimate the stress near a singularity. Another limitation arises as the boundary conditions may not be accurately known, for example the location and nature of the contact between two surfaces may not be known.

It is desirable therefore, especially in safety critical applications such as the aerospace industry, to have another way of determining the stress in the interior of a loaded component independent of any assumptions of boundary or contact conditions. Photoelastic measurement potentially provides such a method and relies on a linear relation between the stress and the permittivity tensor. A casting, or stereolithographic reproduction of the mechanical component is made from a transparent polymer resin. A load is applied to the model while it is slowly heated to its glass transition temperature. When it cools the permittivity tensor retains its anisotropic and inhomogeneous value determined by the stress. When polarized light is transmitted through the model it is observed not to deviate significantly from a straight line path but the polarization state of the emergent light is modified by its encounter with the anisotropic permittivity. The current procedure for three dimensional stress analysis [17, p63][6] is to carefully cut

the model in to thin planar slices. The optical response of each slice is measured using a polarimeter and this used to estimate the difference between the principle stresses in the slice.

A major limitation of this technique is that the model is destroyed and if different load conditions, or a different orientation of slices, is required a new model must be made and the entire procedure repeated. The creation of the sample is time-consuming, for example our own thermal cycling procedure for removing residual stress in a sample takes nine days, the sample must then be stress frozen under load, and then carefully sliced without introducing additional stress. As result this procedure for three dimensional stress analysis is rarely used. It would clearly be advantageous if the full stress tensor could be recovered without destroying the model, which can then be reused under different load conditions and the time consuming and destructive slicing procedure eliminated. The use of photoelastic measurement as a means to retrieve information about internal stresses has been studied extensively: A method known as "Integrated Photoelasticity"[16, 17, 18, 19, 20] has been in use for some time, and it was pointed out[21, 24, 25, 26] that information about the *difference* of principal stress components could be retrieved from appropriate Radon transformations of polarization data. However, these methods do not succeed in reconstructing the stress components separately and therefore the full stress tensor, and the linearly related permittivity tensor, can be obtained in this way only in special cases. Other methods of reconstruction have been suggested, for example, a three-beam measurement scheme[27], where for axisymmetric systems an onion-peeling reconstruction algorithm was proposed[28, 29]. Another method, which in principle is capable of determining a general three-dimensional permittivity tensor and takes account of the non-linearity of the inverse problem, is the "load incremental approach"[22]. Here, the stress on the object is increased in small increments, and at each step, a measurement cycle is performed.

In [10] a method is described and tested numerically which is able recover the five components of the (a small) deviatoric stress from measurements of the polarization state of light. In this paper we demonstrate a numerical procedure, again assuming small stress, to recover all six independent components of the stress at each point in a grid from the polarized light measurements made by apparatus (see Appendix) currently under construction at the University of Sheffield.

2. Elasticity theory

Our component is represented by a bounded connected domain $\Omega \subset \mathbb{R}^3$ with Lipschitz continuous boundary. As a result of forces applied at the boundary the stress $\boldsymbol{\sigma}$, a symmetric rank two tensor field, satisfies the equilibrium condition

$$\sum_{j=1}^{3} \frac{\partial \sigma_{ij}}{\partial x_j} = 0 \tag{1}$$

for each i. Using Cartesian coordinates throughout we will not make a distinction between matrices and rank two tensors. We will have need of the orthogonal decomposition of the space of symmetric $n \times n$ matrices

$$\mathrm{tr}^{-1}0 \oplus \mathrm{tr}^*\mathbb{R} \tag{2}$$

where of course $\mathrm{tr}\mathbf{A} = \sum_{i=1}^{n} a_{ii}$ and $\mathrm{tr}^* t = t\mathbf{1}$, with $\mathbf{1}$ the $n \times n$ identity matrix. When applied to tensor fields this can be regarded as a decomposition in to anisotropic (trace free) and isotropic parts. The projection of a matrix on to the trace free component is $\tau(\mathbf{A}) = \mathbf{A} - (1/n)\mathrm{tr}(\mathbf{A})\mathbf{1}$ so that for any $\mathbf{A}$ the decomposition becomes

$$\mathbf{A} = \tau(\mathbf{A}) + (1/n)\mathrm{tr}(\mathbf{A}). \tag{3}$$

The significance of this decomposition is that any linear map L from the space of symmetric tensors to itself invariant under the action of rotations must preserve this splitting and thus has the form

$$L_{\alpha,\beta}(\mathbf{A}) = \alpha\tau(\mathbf{A}) + \beta\mathrm{tr}(\mathbf{A})\mathbf{1} \tag{4}$$

This is a well known clasical result in tensor analysis, but it can also be seen as an application of Schur's lemma. The orthogonal group acts on symmetric matrices by conjugation, and so the symmetric matrices form a module over the group-algebra.The components in (3) are easily seen to be irreducable submodules, hence any endomorphism of this module must reduce to scalar multiplication on each component. Thus any material property represented by a symmetric tensor field that depends linearly on another such property must have this form (where in general α and β can be scalar fields) if the material response has no preferred direction (that is the material is isotropic). Note that a necessary and sufficient condition for $L_{\alpha,\beta}$ to be invertible is that neither α nor β vanishes and then $L^{-1}_{\alpha,\beta} = L_{\alpha^{-1},\beta^{-1}}$.

Suppose a body undergoes a small deformation represented by the vector field $\mathbf{U}$. The strain tensor $\boldsymbol{\varepsilon}$ is defined by

$$\varepsilon_{ij} = \frac{1}{2}\left(\frac{\partial U_i}{\partial x_j} + \frac{\partial U_j}{\partial x_i}\right) \tag{5}$$

which in geometric terms is (half) the Lie derivative of the of the Euclidean metric with respect to the vector field $\mathbf{U}$, but we will denote (5) in operator form by $\boldsymbol{\varepsilon} = D(\mathbf{U})$. Similarly the equilibrium condition (1) is $D^*\boldsymbol{\sigma} = 0$ where D^* is the formal adjoint. Assuming a linear elastic response we suppose that $\boldsymbol{\sigma} = L(\boldsymbol{\varepsilon})$ for a linear map L. For an isotropic material L must have the form (4), and assuming the material is homogeneous we take the coefficients to be constant. The conventional definition is in terms of the Lamé parameters λ and μ where

$$\boldsymbol{\sigma} = 2\lambda\boldsymbol{\varepsilon} + \mu\mathrm{tr}(\boldsymbol{\varepsilon})\mathbf{1} = L_{\lambda',\mu'}\boldsymbol{\varepsilon} \tag{6}$$

where for convenience $\lambda' = 2\lambda, \mu' = \lambda - 2\mu/3$. The Lamé coefficients are related to the Young's modulus $E > 0$ and Poisson's ratio $\nu \in (-1, 1/2)$ by

$$\lambda = \frac{\nu E}{(1+\nu)(1-2\nu)}, \quad \mu = \frac{E}{2(1+\nu)}. \tag{7}$$

The differential operator D defines an orthogonal splitting (Helmholtz decomposition) of the space of symmetric tensor fields in to the range of D, those that are strain fields for some displacement, and those that are in the kernel of D^* [5]. On a simply connected domain the range of D is also characterized by an integrability condition, the vanishing of the St-Venant compatibility tensor defined by

$$(W\boldsymbol{\varepsilon})_{ijkl} = \frac{\partial^2 \varepsilon_{lj}}{\partial x_i \partial x_k} + \frac{\partial^2 \varepsilon_{ki}}{\partial x_j \partial x_l} - \frac{\partial^2 \varepsilon_{li}}{\partial x_j \partial x_k} - \frac{\partial^2 \varepsilon_{kj}}{\partial x_i \partial x_l} \qquad \text{for } i,j,k,l \in \{1,2,3\} \tag{8}$$

(by symmetry only a subset of 6 the 81 possible choices of (i,j,k,l) are needed for example $(i,j,k,l) \in \{(1,2,1,2),(1,2,1,3),(1,2,2,3),(1,3,1,3),(1,3,2,3),(2,3,2,3)\}$) consequently the equations of linear elasticity

$$\sum_{j=1}^{3} \frac{\partial}{\partial x_j} \left(2\lambda \left(\frac{\partial U_i}{\partial x_j} + \frac{\partial U_j}{\partial x_i} \right) + \mu \sum_{k=1}^{3} \frac{\partial U_k}{\partial x_k} \right) = 0 \tag{9}$$

or more succinctly

$$D^* \left(L_{\lambda',\mu'} D\mathbf{U} \right) = 0 \tag{10}$$

are equivalent on a simply connected domain to the following coupled system [3] with $\mathbf{U}$ eliminated in favour of $\boldsymbol{\varepsilon}$.

$$\boldsymbol{\sigma} = L_{\lambda',\mu'} \boldsymbol{\varepsilon} \tag{11}$$

$$W\boldsymbol{\varepsilon} = 0 \tag{12}$$

Both the stress and strain fields can be split according to (2), the trace free part of the strain is termed the *deviatoric stress* while the trace is termed the *hydrostatic stress*. In many practical applications it is the deviatoric strain that is more important. Solid metals typically have a high bulk modulus so that hydrostatic stress results in small reversable volume changes, and is not relevant in the prediction of failure of mechanical components. The Tresca yield criteria is that the difference of the maximum and minimum principle stresses at a point exceeds a certain threshold while von Mises yield criterion is reached when the frobenius norm of the deviatoric stress exceeds a threshold. Both depend only on the deviatoric stress. However criteria for fracture may require the full stress tensor.

The relation between the permittivity tensor and the stress and strain is assumed to be linear, and assuming the material to be homogeneous, must be of the form (4). It is traditionally quoted as a 'stress optical law' (13), although under the assumptions of linear elasticity one could equally well quote a strain optical law.

$$\boldsymbol{\epsilon} = L_{C_0,C_1}(\boldsymbol{\sigma}) \tag{13}$$

In photoelastic tomography we will use this relation to recover the deviatoric component of the stress from the trace free component of the permittivity tensor. Direct measurement of the trace of the permittivity requires a more complicated measurement apparatus as we see in section 4, and for this reason typically only values for C_0 are quoted in the literature for various materials.

3. Ray approximation and uniqueness of solution

We begin with the following formulation of Maxwell's equations

$$\nabla \times \mathbf{H} + \mathrm{i}\omega\boldsymbol{\epsilon}\mathbf{E} \ = 0 \tag{14}$$

$$\nabla \times \mathbf{E} - \mathrm{i}\omega\mu_0\mathbf{H} = 0 \tag{15}$$

Where $\mathbf{E}$ and $\mathbf{H}$ are complex vector fields representing spatially the electric and magnetic fields respectively, the time variation being given in both cases by multiplication by $\mathrm{e}^{\mathrm{i}\omega t}$ and taking the real part. We take the permeability to be isotropic and to have the constant (free space) value μ_0, whereas the permittivity $\boldsymbol{\epsilon}$ is anisotropic and in general inhomogeneous.

We have Given an isotropic homogeneous permittivity $\epsilon_1\mathbf{1}$ we suppose that the stressed component results in a possibly anisotropic permittivity $\boldsymbol{\epsilon} = \epsilon_1\mathbf{1} + \boldsymbol{\eta}$, where $\mathrm{supp}\boldsymbol{\eta} \subset \Omega$.

The assumption Kratsov [13] terms *quasi-isotropic*, that in addition to the anisotropy $\tau\boldsymbol{\eta}$ being small, its spatial derivatives are also small, yields a ray optics approximation as described below. A summary of the conditions for the validity of this approximation in terms of heuristic length scales is given in [10], and the approximation is derived as an asymptotic expansion in [2], see also [14],[15]. Let γ be the ray (oriented line) $\{\mathbf{x}_0 + s\mathbf{v} : s \in \mathbb{R}\}$ with $|\mathbf{v}| = 1$, we define P_γ be the projection of vector in $\mathbb{R}^3$ on the subspace perpendicular to $\mathbf{v}$, and by extension the projection of a symmetric matrix. Explicitly $P_\gamma(\mathbf{w}) = \mathbf{w} - (\mathbf{w}\cdot\mathbf{v})\mathbf{v}$. In the ray approximation the (complex) electric field $\mathbf{E}$ propagating along the ray γ satisfies the system of ordinary differential equations (Rytov's law)

$$\frac{\partial}{\partial s}\mathbf{E} = \frac{\mathrm{i}}{2\epsilon_1}P_\gamma(\boldsymbol{\epsilon}\mathbf{E}) \tag{16}$$

and $\mathbf{E}\cdot\mathbf{v} = 0$. A simple calculation shows that $\partial|\mathbf{E}|^2/\partial s = 0$, hence a solution operator U defined by $\mathbf{E}(s_1) = T\mathbf{E}(s_0)$ is unitary. Here s_1 and s_0 are chosen so that $\mathbf{x_0} + s_i\mathbf{v}$ are outside $\bar{\Omega}$, and correspond to the location of light source and measurement system. Let us assume for the moment that we are able, for each γ to arrange for $\mathbf{E}(s_0)$ to be a spanning set for the set of complex vectors orthogonal to $\mathbf{v}$ and measure the emerging electric field $\mathbf{E}(s_1)$. Choosing a basis arbitrarily for the plane normal to $\mathbf{v}$ we can represent our data as a unitary 2×2 matrix T_γ for each γ, and from this data we seek to recover $\boldsymbol{\eta}$. Note that for the ray with the opposite orientation, which we will denote by $-\gamma$, the data is simply the inverse $T_{-\gamma} = T_\gamma^*$.

One can interpret the data as a section of a suitable fibre bundle as we shall describe. Although this is not essential for a basic understanding of the problem, it is convenient

to formulate the data space in this way rather than as a matrix for each ray as there is no continuous assignment of basis vectors to all two dimensional subspaces of $\mathbb{R}^3$ and that makes discussion of global smoothness and norms of the data difficult in a local basis.

We can identify the set of rays in $\mathbb{R}^3$ with the tangent bundle to the unit sphere $S^2 \subset \mathbb{R}^3$. The ray γ parameterized by $\mathbf{x}_0 + s\mathbf{v}$ (with $\mathbf{x}_0$ chosen to have minimum norm so as to be unique) is identified with $\mathbf{x}_0 \in T_{\mathbf{v}}S^2$, a point in the tangent space to the sphere at $\mathbf{v} \in S^2$. Our data thus assigns unitary operator T_γ each point on $\gamma \in TS^2$, acting on the complexification of $T_{\mathbf{v}}S^2$, a section of a $U(2)$ bundle over the total space TS^2. We will denote the bundle by $\mathcal{U}$. Of course from the symmetry of the data one need only consider one of γ and $-\gamma$ so one could formulate the data as a function of non-oriented lines. Below when we linearize the problem, a perturbation in our data will live in a Lie algebra $\mathfrak{u}(2)$ bundle over TS^2, more specifically the linearized data will be imaginary symmetric, so we will denote the bundle of symmetric real matrices over TS^2 by Σ.

Anisotropic inverse boundary value problems for Maxwell's equations are in their infancy, and one might compare the current situation to the state of knowledge of the isotropic low frequency problem of electrical impedance tomography at the time of Calderón's foundational paper in 1980 [23]. We have very little idea about uniqueness of solution even for this quasi-isotropic approximation but we can understand linearized problem, about a constant background fairly completely. The state of the art is summarized by the following results of Sharafutdinov. We define a forward mapping by $F : C^\infty(\mathcal{S}^2\Omega) \to C^\infty(\mathcal{U})$, $F_\gamma(\eta) = T_\gamma$ (where $\mathcal{S}^2\Omega$ denotes the bundle of symmetric rank 2 tensors over the domain Ω). Sharafutdinov derives a Neumann series for F , and this can easily extended along the lines used by [23] to a proof that F is analytic at 0, and its Fréchet derivative is the *transverse ray transform* of $\boldsymbol{\eta}$

$$F'_\gamma(\boldsymbol{\eta}) = \frac{\mathrm{i}}{2\epsilon_1} \int_\gamma P_\gamma(\boldsymbol{\eta})\, ds =: R[\boldsymbol{\eta}]. \tag{17}$$

Just as the Radon transform it can be extended to distributions. Sharafutdinov [2] shows that the transverse Ray transform $R : H^1(S^2\Omega) \to H^1(\Sigma)$ is injective and there is a constant C such that

$$||\boldsymbol{\eta}||_0 < C||R[\boldsymbol{\eta}]||_1. \tag{18}$$

Here the prefix H^1 indicates the Sobolev space of sections of a bundle. The proof is closely related to the inversion of the scalar Radon transform as we shall explore further below. While (18) gives a stability result for the inverse problem not that it is not sufficient to justify the use of the Inverse Function Theorem on Banach spaces to deduce a local uniqueness result for the nonlinear inverse problem. In particular the range of F' is not closed.

The reduction of the inversion of the transverse ray transform to a scalar Radon transform is instructive. It gives a subset of the data sufficient to recover the permittivity

tensor, as well as giving an explicit reconstruction algorithm. From the point of view of our experimental apparatus, to consider the rays corresponding to one 'projection', that is perpendicular to one plane, together as the plane represent the plane of camera. The reduction to the scalar Radon transform begins by considering all rays in one plane, normal to a vector $\mathbf{n}$. For the rays in this plane we consider only the data corresponding to an incident electric field in the $\mathbf{n}$ direction and measurement of the outgoing field in the same direction.

$$\mathbf{n} \cdot F'_\gamma(\boldsymbol{\eta})\mathbf{n} = \frac{\mathrm{i}}{2\epsilon_1} \int_\gamma \mathbf{n} \cdot \boldsymbol{\eta}\mathbf{n}\, ds \tag{19}$$

This is simply a scalar Radon transform of the function $\mathbf{n} \cdot \boldsymbol{\eta}\mathbf{n}$ and thus can be inverted using filtered back-projection as used in traditional X-ray CT. It is natural, following the traditional configuration of a computerised axial tomograph, to consider data only from rays parallel to one fixed plane, for example horizontal rays. Applying (19) with $\mathbf{n} = \mathbf{e}_3 = (0\,0\,1)^T$ gives a reconstruction of ϵ_{33}. To recover all the components of ϵ by this method one must consider planes normal to six vectors $\mathbf{n}_i$ such that $\{\mathbf{n}_i\mathbf{n}_j^T + \mathbf{n}_j\mathbf{n}_i^T | i, j = 1, 2, 3\}$ spans the space of symmetric 3×3 matrices. For example $\{\mathbf{e}_1, \mathbf{e}_2, \mathbf{e}_3, \mathbf{e}_1 + \mathbf{e}_2, \mathbf{e}_2 + \mathbf{e}_3, \mathbf{e}_3 + \mathbf{e}_1\}$ is one possible choice. Rather than rotating the measurement apparatus through 90° and 45° it more convenient simply to rotate the specimen, a 45° (or less) rotation being provided by a transparent wedge. Reconstructions of simulated data using this method were presented in [10]. Note that while this gives argument gives an example of sufficient data, it appears somewhat wasteful as for each of the six configurations of the data only one of the three possible measurements along each ray is used and the others discarded. The possibility exists therefore that less than six configurations, but using the complete data for each ray, may be sufficient. We explore this possibility numerically in section 5.

4. Photoelastic measurements

Unfortunately a conventional polariscope cannot measure the complete optical response of the material. Consider a fixed ray γ and basis for the plane perpendicular to the ray. The complete optical response for a fixed frequency of light is the matrix $T_\gamma \in U(2)$. A factorization of a unitary matrix, detailed in [9] gives a chart on $SU(2)$. Let $R(\theta)$ be the real rotation matrix throught an angle θ

$$R(\theta) = \begin{bmatrix} \cos\theta & \sin\theta \\ -\sin\theta & \cos\theta \end{bmatrix}$$

and define

$$G(\theta) = \begin{bmatrix} \mathrm{e}^{\mathrm{i}\theta} & 0 \\ 0 & \mathrm{e}^{-\mathrm{i}\theta} \end{bmatrix}$$

then any $U \in SU(2)$ can be written as

$$U = R(\alpha)G(\Delta)R(-\beta) = \cos\Delta\, R(\alpha - \beta) + \mathrm{i}\sin\Delta \begin{bmatrix} \cos(\alpha+\beta) & \sin(\alpha+\beta) \\ \sin(\alpha+\beta) & -\cos(\alpha+\beta) \end{bmatrix} \tag{20}$$

(consider names for angles). When U is the transfer matrix of an optical system the parameters in (20) are termed *characteristic parameters of photoelasticity*, specifically α is the primary and β the secondary principal directions and Δ the retardation. These can be conveniently and accurately measured by our polariscope. An arbitrary matrix in $U(2)$ can be obtained by multiplication by $\pm e^{i\phi/2}$ resulting in a matrix with determinant $e^{i\phi}$, and in the optical context ϕ is a change in phase of the light passing through our system. This phase is much more difficult to measure, as it corresponds to measuring distances on the scale of a wavelength of light. Typically such measurements would be achieved by interferometry.

Photoelastic data therefore comprises of unitary matrices scaled to have a unit determinant. Let $h(U) = \pm\frac{1}{\sqrt{\det U}}U$ then $h : U(2) \to SU(2)/\mathbb{Z}_2$ (a Lie group homomorphism) takes a unitary matrix to the equivalence class of special unitary matrices 'ignoring sign' and reduces complete data to photoelastic data. As one might expect this reduction in data means that one cannot completely recover the (perturbation in) the permittivity tensor. This loss of information can be observed directly in Rytov's law. Let $\boldsymbol{\epsilon} = \tilde{\boldsymbol{\epsilon}} + \zeta\mathbf{1}$ where $\operatorname{tr}\tilde{\boldsymbol{\epsilon}} = 0$

$$\frac{\partial}{\partial s}\mathbf{E} = \frac{\mathrm{i}}{2\epsilon_1}P_\gamma\left(\left(\tilde{\boldsymbol{\epsilon}} + \zeta\mathbf{1}\right)\mathbf{E}\right) \tag{21}$$

so that

$$\left(\frac{\partial}{\partial s} - \frac{\mathrm{i}\zeta}{2\epsilon_1}\right)\mathbf{E} = \frac{\mathrm{i}}{2\epsilon_1}P_\gamma\left(\tilde{\boldsymbol{\epsilon}}\mathbf{E}\right). \tag{22}$$

Now defining $\tilde{\mathbf{E}} = \exp(-\mathrm{i}\zeta s/2\epsilon_1)\mathbf{E}$ we have

$$\frac{\partial\tilde{\mathbf{E}}}{\partial s} = \frac{\mathrm{i}}{2\epsilon_1}P_\gamma\left(\tilde{\boldsymbol{\epsilon}}\tilde{\mathbf{E}}\right). \tag{23}$$

Taking $\tilde{T}_\gamma(s)$ to be the solution operator for (23) so that $\tilde{\mathbf{E}}(s) = \tilde{T}_\gamma\tilde{\mathbf{E}}(s_0)$ clearly $\partial\det\tilde{T}_\gamma/\partial s = 0$ so that $\det\tilde{T}_\gamma(s) = 1$ for all s. In particular we denote $\tilde{T}_\gamma(s_1)$ simply by $\tilde{T}_\gamma$. As a consequence of this change of variables, we see that the equivalence class of permittivity tensors differing by an isotropic tensor gives rise to an equivalence class of measurements T_γ determined up to multiplication by a unit complex number.

Sharafutdinov defines the truncated transverse ray transform as the the Ray transform defined earlier projected on to trace-free matrices and shows that this is the linearization of the data obtained from (23). In particular the perturbation in $\tilde{T}_\gamma$ will be a trace-free imaginary matrix. From such a trace free matrix one can recover the anisotropic part of $\boldsymbol{\eta}$, the isotropic part forming the null space of the truncated transverse ray transform. We see therefore that using conventional photoelastic data the deviatoric component of the stress is determined uniquely and with the same stability estimate as (18). If the deviatoric part is all that is needed one could apply the inverse Radon transform method of Sharafutdinov (with only five rotation axes $\mathbf{n}$), or a regularized algebraic solution of the truncated ray transform.

In some cases the isotropic (that is hydrostatic) stress is required and clearly some additional equations are required. In the case where the body forces are zero in the

interior the equilibrium equation is sufficient to determine the hydrostatic stress up to single additive constant. To see this suppose $\boldsymbol{\sigma} = \tilde{\boldsymbol{\sigma}} + p\mathbf{1}$ where $\operatorname{tr} \tilde{\boldsymbol{\sigma}} = 0$, then from the equilibrium equations (1) becomes

$$-\sum_{j=1}^{3} \frac{\partial \tilde{\sigma}_{ij}}{\partial x_j} = \frac{\partial p}{\partial x_i} \tag{24}$$

so the gradient of p is known and hence as Ω is assumed connected p is determined up to an added constant. The constant could be determined by additional data, for example the work done in loading the sample.

5. Numerical implementation and results

5.1. Discrete appoximation to Ray Transform

A cubic grid of N^3 voxels was was defined on cube containing Ω. For each projection we assumed the camera plane was divided in to $M_1 \times M_2$ pixels. For each axis of rotation L angular increments were considered, and $K \leq 6$ axes of rotation were used. The length of the intersection of rays with voxels was calculated using the fast algorithm of Jacobs *et al*[12], and the resulting matrix of the scalar Radon transform combined with rotations and projections to produce a discrete approximation to the transverse and truncated transverse ray transform as a $3M_1M_2LK \times 6N^3$ matrix $\mathbf{R}$.

To study the rank of the discrete approximation to the ray transform for a variety of number of angular steps and rotations of axis we assembled the matrix in matlab using sparse storage.

By contrast for realistic values of M_1, M_2 and L (and N chosen so that voxels are of similar size to camera pixels) the matrix generated is too large to store convieniently even using sparse storage, so we implemented functions in matlab to multiply a vector by $\mathbf{R}$ or $\mathbf{R}^T$ calculating elements of the matrix as needed. In practise it is more convenient to generate the elements of the matrix by rows, following the path of each ray through the voxels. Consequently we implement the product $\mathbf{z} = \mathbf{R}^T\mathbf{y}$ by acumulation of $R_{ji}y_j$ in the variable $\mathbf{z}$ for each j in turn.

5.2. Singular value studies

To generate the singular value decomposition of $\mathbf{R}$ we used a coarse discretization of the object into $9 \times 9 \times 9$ voxels resulting in matrices of sizes ranging from 58320×4374 (4 degree steps) to 15552×4374 (15 degree steps). As expected the decay of the singular values shows that the inverse problem is only mildly ill-posed, as expected from the SVD of the scalar Radon transform [8]. In figure 1 we consider first only one axis of rotation, and about this axis we rotate the plane of the camera in 25, 15 an 5 degree increments in turn. It is seen that increasing the number of measurement increases the number of unknowns we expect to be able to recover reliably with a maximum approaching five degrees of freedom per voxel (3645). With a course mesh there are some errors in

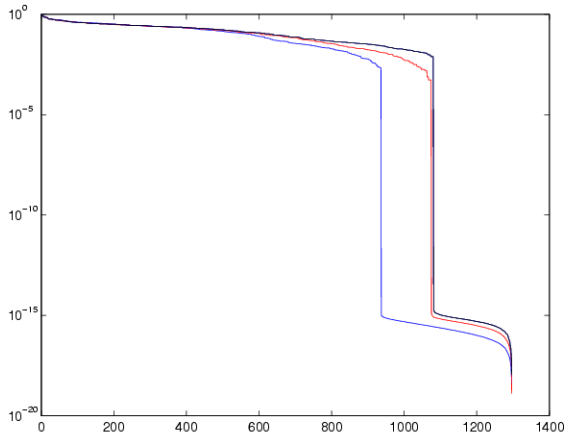

Figure 1. The singular values on a logarithmic scale for one axis of rotation, with 25, 15 and 5 degree increments of rotation. It is seen that increasing the number of measurements increases the number of unknowns we expect to be able to recover reliably with a maximum approaching five degrees of freedom per voxel

the discretization due complications due to intersection of rays with corner and edge pixels. The regulaized matrix has an effective rank of 4274 rather than teh expected $9^3 \times 6 = 4374$. Surprisingly the singular values suggest that with sufficiently accurate data all five components of the deviotoric stress can be recovered from measurements using only one axis of rotation. This not contradic the result that six axes are *suffcient*, and notice that in the reduction to a scalar Radon transform not all elements the δT_γ matrices were used. However one should always be cautious in interpreting singular values without considering the singular vectors. Our attempts at reconstruction with only one axis confirm that the five components are not recovered with the same accuracy over all voxels. One interpretation is that with only one axis but with the whole matrix we could synthesise limited angle tomography data for planes not perpendicular to the axis of rotation, as data is collected along rays in such a plane only where they intersect with the plane of the camera.

Now considering the effect of using five axes of rotation, specifically $\mathbf{n} \in \{\mathbf{e}_2, \mathbf{e}_3, \mathbf{e}_1 + \mathbf{e}_2, \mathbf{e}_2 + \mathbf{e}_3 + \mathbf{e}_1 + \mathbf{e}_3\}$. We (figure 2) that although the rank of the matrix is the same, the condition number of the matrix truncated at any given singular component is improved.

5.3. Elastic regularization

From the decay of the singular values w see that some regularization is needed to implement an *a priori* smoothness constraint on the solution. If classical filtered backprojection is used[8], each component $\mathbf{n} \cdot \boldsymbol{\sigma} \mathbf{n}$ will be "smoothed" separately, however the elasticity equations imply relations between the derivatives of different components.

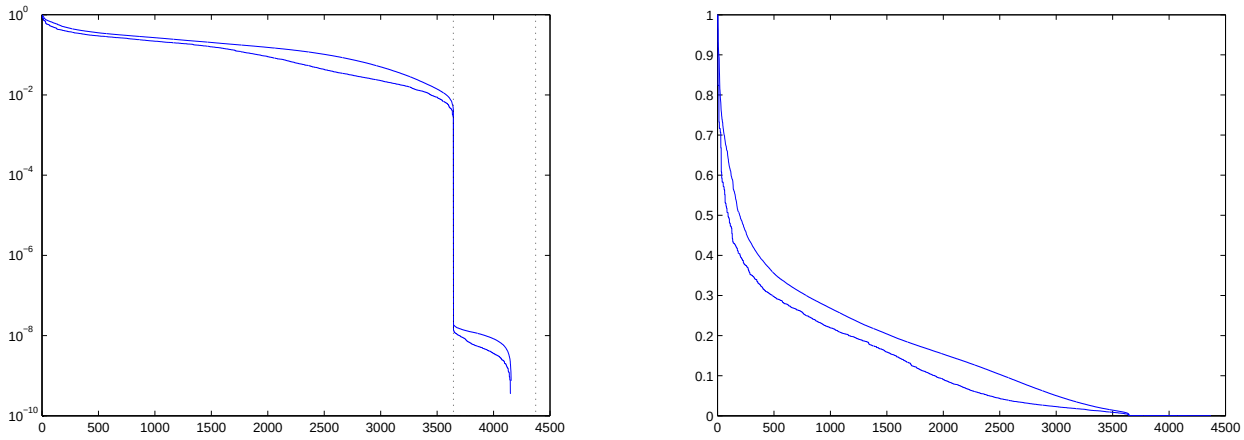

(a) (b)

Figure 2. The singular values on a logarithmic scale (a) and linear scale (b) with one axis (lower trace) and five axes (upper trace). The efective rank of the matrix is seen to be the same but that increasing the number of axes improves the condition number.

We propose the following *elastic regularization* scheme where we minimize

$$\|\mathbf{R}L_{C_0^{-1},0}\boldsymbol{\sigma} - d\|^2 + a^2\|\mathbf{D}^*\boldsymbol{\sigma}\|^2 + b^2\|\mathbf{W}L_{\lambda'^{-1},\mu'^{-1}}\boldsymbol{\sigma}\|^2$$

Here $\mathbf{R}$ is the discrete truncated transverse ray transform for 5 axes, $\mathbf{D}^*\boldsymbol{\sigma}$ is a finite difference approximation to the operator in the equilibrium equation (1), $\mathbf{W}$ is a finite difference approximation to the St-Venants compatibility operator, $\mathbf{d}$ is the data δT_γ assembled in a vector, and a and b are regularization parameters that control the trade-off between fitting the data and satisfying the *a priori* assumptions. The solution to this minimization problem is also the least squares solution of the augmented linear system

$$\begin{bmatrix} \mathbf{R}L_{C_0^{-1},0} \\ a\mathbf{D}^* \\ b\mathbf{W}L_{\lambda'^{-1},\mu'^{-1}} \end{bmatrix} \boldsymbol{\sigma} = \begin{bmatrix} \mathbf{d} \\ \mathbf{0} \\ \mathbf{0} \end{bmatrix} \tag{25}$$

Using the course discretization described in the previous section we calculated the singular values of the agmented matrix, as well as the condition number of the matrix being improved by increase in a and b, we also see that as expected the addition of the equilibrium equations has resulted in an increase in the effective rank to nearly six per voxel.

5.4. Reconstruction of simulated data

To generate test examples with zero body force we use a classical analytic solution of (9). Following [1] we take four harmonic functions $\phi_i, i = 0, ..., 3$, $\nabla^2\phi_i = 0$ and construct a

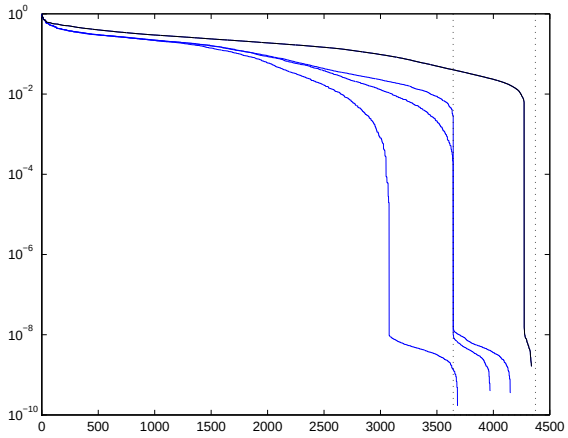

Figure 3. The upper curve is the singular values of the ray transform augmented by the elastic regularization matrices (equilibrium and compatibility). Note that the rank is now almost 6 per voxel.

displacement field

$$U_i = \phi_i - \alpha \left(\phi_0 + \sum_{j=1}^{3} x_j \phi_j \right)$$

which then satisfies (9) provided

$$\alpha = \frac{\lambda + 4\mu/\lambda}{4(\lambda + 2\mu)}.$$

We therefore choose polynomials for each ϕ_i to generate a non-trivial test case.

In contrast to [10] in which Rytov's law (16) is solved using a numerical ODE solver we used the linear approximation to generate the data, which of course is valid for sufficiently small $\boldsymbol{\eta}$. However to avoid 'inverse crimes' the simulated data was generated on a $15\times15\times15$ grid while the reconstruction performed on a $9\times9\times9$ grid, and simulated noise was added to the data using a pseudo random number generator. The level of noise chosen was approximately that expected in the measurement system described in the Appendix and was independent Gaussian distribution with a standard deviation of 0.23 degrees.

The augmented linear system (25) was solved using the Conjugate Gradient Least Squares (CGLS) algorithm [30, Ch 7]. Note that requires one multiplication by of a vector $\mathbf{R}$ and one by $\mathbf{R}^T$ for each iteration. The iteration was stopped when the residual error in the predicted data fell below a predetermined level. The results were displayed using the Mayavi visualization program. Figure 4 shows plots of the principle axes of the original stress tensor at selected points from three viewpoints and figure 5 our reconstruction.

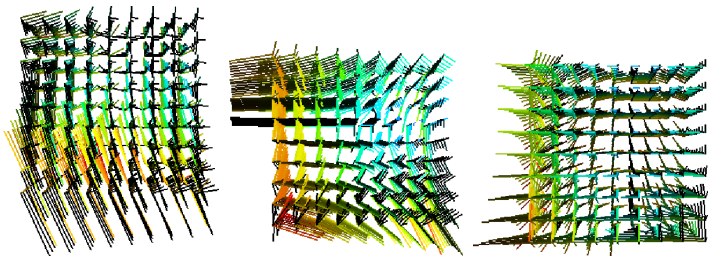

(a) x (b) y (c) z

Figure 4. Original tensor field represented (using MayaVi) by line segments for each eigenvector with length proportinal to the eigenvalue, from three differnt views

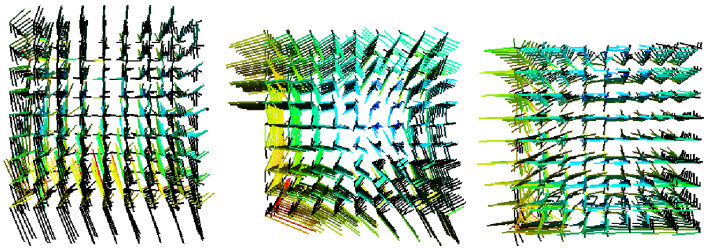

(a) x (b) y (c) z

Figure 5. Reconstructed tensor field with the same representation

6. Conclusions

In this study we have presented a numerical method for reconstructing the deviatoric stress (under the assumption that the stress is small) from photoelastic measurements , and the full stress tensor in the absence of body forces. While theory tells us that measurements from five rotation axes are sufficient to recover the deviatoric stress tensor, the singular values of the forward operator indicate that much of the information is contained in the data from one axis. Our reconstruction method can be implemented using sparse matrix techniques and so we expect it to scale well to realistic sized problems. The application of this method to real data is still work in progress and we expect to be able to compare this matrix based method with the Radon transform inversion method described in [10]. We anticipate for some stress distributions encountered in practice the linear approximation used in this paper will not be adequate, and that a Newton-Kantorovich method including a numerical solution of Rytov's law will be required.

In the method reported in this paper the regularization employed rather than an ad-hoc penalty term we derived from a physical condition loosely enforced. We note that this idea is relevant to a range of inverse problems where inaccurately known physical constraints provide a regularizing penalty term.

Appendix: Measurement system

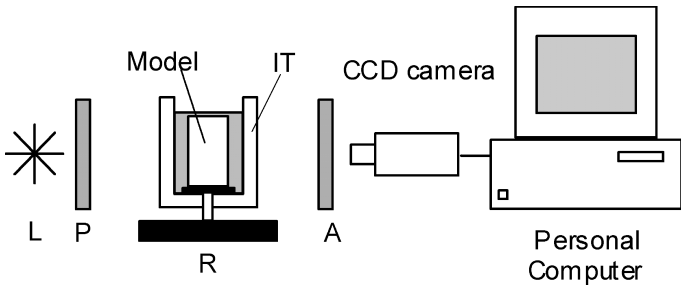

Figure 6. The measurement system illustrating the light source L, polariser P, Analyser A, Rotation stage R and Immersion Tank IT.

We felt a brief description of the measurement apparatus under construction in Sheffield would help the reader understand the physical motivation for this problem. The apparatus in figure 6, consists of a three-dimensional birefringent model placed within a standard transmission plane polariscope in a transparent tank containing an immersion fluid of equivalent refractive index to the model. The polariscope consists of a collimated laser light source, two polarisers (known as the polariser and analyser) and a CCD camera, of 256×320 pixels.

The tank is made of stress free glass and has parallel sides so that the light is not refracted as it passes through the tank. It is more convenient to rotate the sample than the light source and polariscope and this is achieved by the rotating stage inside the tank which is coupled via a sealed bearing to a precision rotation stage mounted under the tank. The CCD camera, polarisers, and rotation stage are all controlled via the personal computer and thus their operation can be synchronised. The rotation stage provides rotations about the vertical axis with a resolution of 0.001 degrees, an origin repeatability of 0.001 degrees, an absolute accuracy of 0.023 degrees and a maximum speed of 20 degrees/second. It is possible that data will be recorded for every 5 degrees of rotation, through 180 degrees. Discrete rotations about horizontal axes are achieved by manually turning the specimen through 90 degrees or by placing the specimen on a wedge, made of transparent material with the same refractive index as the matching fluid, resulting in a rotation of 45 degrees or less.

A Fourier polarimetry method [31] is used to obtain the photoelastic characteristic parameters for each view of the model. The polariser and analyser are rotated to discrete positions during a 360° revolution of the polariser, this is usually 72 positions, and at each position an image can be captured using the automated CCD camera. The analyser is rotated to an angle three times the angle of the polariser, so that the analyser rotates three times during one rotation of the polariser. Alternative and faster rotation ratios may also be used. The intensity images then recorded can be considered to be one period of an infinite signal and as a result can be represented using a Fourier series. A program was written which uses a Fourier transform and the intensity images to find the Fourier coefficients of the Fourier series. Using the Stokes vector and Mueller matrix

representations the equations that relate the Fourier coefficients to the characteristic parameters.

The automated system rotates the model, then for each view the automated polarimetry system determines the characteristic parameters for each pixel of the camera (320 x 256) and the data recorded on the computer. A full measurement cycle is expected to take 259 minutes (72 images at 1 image per second, 36 increments (i.e. every 5 degrees), 6 orientations) excluding the time taken for manual re-positioning about horizontal axes, and the data collected will occupy approximately ??MBytes.

A detailed description of this apparatus together with the results of applying the algorithm reported here to experimental results will be reported in a subsequent paper[11]

Acknowledgements

We like to thank James Montaldi, David Harris and Andrew Reader for helpful discussions. This work is supported by EPSRC grants numbers GR/R86300 and GR/R86270.

References

[1] S.P. Timoshenko and J.N. Goodier Theory of Elasticity, 3rd edition, McGraw-Hill (1951)

[2] V.A. Sharafutdinov, Integral Geometry of Tensor Fields, Inverse and Ill-Posed Problems Series, VSP, Utrecht, the Netherlands, 1994.

[3] P.G. Ciarlet, P. Ciarlet Jr., Another approach to linearized elasticity and Korn s inequality, C. R. Acad. Sci. Paris, Ser. I 339, 2004,.

[4] E. G. Coker and L. N. G. Filon, Photo-Elasticity, Cambridge University Press, Cambridge, 1957, edition2nd ed..

[5] M Berger, D Ebin, Some decompositions of the space of symmetric tensors on a Riemannian manifold. J. Differential Geometry 3 1969 379–392.

[6] H.Fessler,, An assessment of frozen stress photoelasticity, J. Strain Analysis, 27 (3), 123-126, 1993.

[7] RA Tomlinson, EA Patterson, The Use of Phase-Stepping for the Measurement of Characteristic Parameters in Integrated Photoelasticity, Experimental Mechanics, Vol. 42, No. 1, 43-50 (2002).

[8] F. Natterer, The mathematics of computerized tomography, Society for Industrial and Applied Mathematics, Philadelphia , 2001.

[9] H Hammer, Characteristic parameters in integrated photoelasticity, an application of Pincaré's eqivalence theorem, J Mod Opt 51, 597-618 (2004).

[10] H Hammer, W. R. B. Lionheart Reconstruction of spatially inhomogeneous dielectric tensors through optical tomography JOSA A, Vol. 22, 250, 2005

[11] RA Tomlinson, H Yang, D Szotten, WRB Lionheart, The Design and Commissioning of a Novel Tomographic Polariscope, in preparation.

[12] F. Jacobs, E. Sundermann, B. De Sutter, M. Christiaens and I. Lemahieu A Fast Algorithm to Calculate the Exact Radiological Path through a Pixel or Voxel Space Journal of Computing and Information Technology, - CIT 6, 1998, 1, pp. 89-94

[13] Y. A. Kravtsov, Dokl. Akad. Nauk. SSSR, 183, 74,1968.

[14] Y. A. Kravtsov and Y. I. Orlov, Geometric Optics of Inhomogeneous Media, Nauka, Moscow, 1980).

[15] A. A. Fuki, Y. A. Kravtsov and O. N. Naida, Geometrical Optics of Weakly Anisotropic Media, Gordon and Breach Science Publishers,Amsterdam, 1998.
[16] H. K. Aben, Optical phenomena in photoelastic models by the rotation of principal axes, Exp. Mech. 6, 13 22 (1966).
[17] H. Aben, Integrated Photoelasticity (McGraw-Hill, New York, 1979).
[18] H. K. Aben, J. I. Josepson, and K.-J. E. Kell, The case of weak birefringence in integrated photoelasticity, Opt. Lasers Eng. 11, 145 157 (1989).
[19] H. Aben and C. Guillemet, Photoelasticity of Glass (Springer-Verlag, Berlin, 1993).
[20] H. Aben and A. Puro, Photoelastic tomography for three dimensional flow birefringence studies, Inverse Probl. 13, 215 221 (1997).
[21] M. Davin, Sur la composition des petites biréfringences subies par un rayon traversant un modèle photoélastique faiblement contraint, C.R. Seances Acad. Sci. Ser. A 269, 1227 1229 (1969).
[22] M. L. L. Wijerathne, K. Oguni, and M. Hori, Tensor field tomography based on 3D photoelasticity, Mech. Mater. 34, 533 545 (2002)
[23] Calderón AP, 1980, On an inverse boundary value problem. In Seminar on Numerical Analysis and Its Applications to Continuum Physics, pp. 67-73, Rio de Janeiro, Sociedade Brasileira de Matematica.
[24] H. Aben, S. Idnurm, and A. Puro, Integrated photoelasticity in case of weak birefringence, in Proceedings of the 9th International Conference on Experimental Mechanics (ICEM, Copenhagen, 1990), Vol. 2, pp. 867 875.
[25] H. Aben, S. Idnurm, J. Josepson, K.-J. Kell, and A. Puro, Optical tomography of the stress tensor field, in Analytical Methods for Optical Tomography, G. G. Levin, ed., Proc. SPIE 1843, 220 229 (1991).
[26] H. Aben, A. Errapart, L. Ainola, and J. Anton, Photoelastic tomography in linear approximation, in Proceedings of the International Conference on Advanced Technology in Experimental Mechanics, 2003
[27] Y. A. Andrienko and M. S. Dubovikov, Optical tomography of tensor fields: the general case, J. Opt. Soc. Am. A 11, 1628 1631 (1994).
[28] Y. A. Andrienko, M. S. Dubovikov, and A. D. Gladun, Optical tomography of a birefringent medium, J. Opt. Soc. Am. A 9, 1761 1764 (1992).
[29] Y. A. Andrienko, M. S. Dubovikov, and A. D. Gladun, Optical tensor field tomography: the Kerr effect and axisymmetric integrated photoelasticity, J. Opt. Soc. Am. A 9, 1765 1768 (1992).
[30] Å. Björck, Numerical Methods for Least Squares Problems, SIAM, Philadelphia, 1996.
[31] H. Yang, S. Gibson and R. A. Tomlinson, Development of Fourier Polarimetry for 3D photoelasticity, submitted to Experimental Mechanics.